Potassium titanyl phosphate: properties and new applications

John D. Bierlein and Herman Vanherzeele

Central Research & Development Department, E. I. du Pont de Nemours & Company, Inc., Wilmington, Delaware 19880-0356

Received October 3, 1988; accepted December 16, 1988

Potassium titanyl phosphate (KTP) is a unique nonlinear-optical material that is being widely used for second-harmonic generation of Nd lasers emitting near 1 μm. KTP is also attractive for various sum- and difference-frequency and optical parametric applications over its entire transparency range from 0.35 to 4.5 μm. Its combination of large electro-optic coefficients and low dielectric constants makes KTP potentially useful for various electro-optic applications, and, in particular, it has a figure of merit for an optical waveguide modulator that is nearly a factor of 2 larger than that for any other inorganic material. Low-loss optical waveguides can be formed in KTP, and several electro-optic and nonlinear-optic devices have been fabricated that confirm that KTP is also a superior material for many optical waveguide applications.

1. INTRODUCTION

Potassium titanyl phosphate ($KTiOPO_4$; KTP) is a relatively new material that has been shown to have superior properties for several nonlinear-optical applications and, in particular, for frequency doubling the 1-μm radiation of Nd lasers.[1,2] Its high nonlinear-optical d coefficients, high optical damage threshold, wide acceptance angles, and thermally stable phase-matching properties make it useful for this purpose, and its large linear electro-optic r coefficients and low dielectric constants make it attractive for various electro-optic applications, such as modulators and Q switches.[3] KTP also has an electro-optic waveguide modulator figure of merit that is nearly double that for any other inorganic material.[3] Recently low-loss optical waveguide fabrication processes were developed for KTP that, together with its large figure of merit, suggest that this material is also promising for integrated-optic applications.[4] This paper reviews the basic characteristics of KTP, such as crystal structure and crystal growth (Section 2), linear and nonlinear-optical properties, including various new frequency-conversion applications in bulk material (Section 3), electro-optic and dielectric properties (Section 4), optical waveguide fabrication processes and characteristics (Section 5), and, finally, new nonlinear-optical applications and optical waveguide device properties (Section 6).

2. STRUCTURE AND CRYSTAL GROWTH

KTP belongs to the family of compounds that have the formula unit $MTiOXO_4$, where M can be K, Rb, Tl, NH_4, or Cs (partial) and X can be P or As. Solid solutions exist among the various members of this family, with only slight changes in lattice parameters. All members are orthorhombic and belong to the acentric point group mm (space group $Pna2_1$). For KTP the lattice constants are $a = 12.814$ Å, $b = 6.404$ Å, and $c = 10.616$ Å, and each unit cell contains eight formula units. The structure is characterized by chains of TiO_6 octahedra, which are linked at two corners, and the chains are separated by PO_4 tetrahedra (see Fig. 1).[5] There are two chains per unit cell, and the chain direction alternates between [011] and [0$\bar{1}$1]. Alternating long and short Ti–O bonds occur along these chains, which result in a net z-directed polarization and are the major contributor to KTP's large nonlinear-optic and electro-optic coefficients. The K ion sits in a high-coordination-number site and is weakly bonded to both the Ti octahedra and P tetrahedra. Channels exist along the z axis ([001] direction) whereby K can diffuse (through a vacancy mechanism) with a diffusion coefficient several orders of magnitude greater than in the x–y plane.

KTP decomposes on melting ($\simeq$1150°C), and hence normal melt processes cannot be used to grow this material. However, large single crystals of KTP can be grown by both hydrothermal and flux techniques. The hydrothermal process has been commercialized and consists of sealing nutrient and seed crystals in a Au tube, inserting the tube into a high-pressure–high-temperature autoclave and growing crystals at constant pressure ($\simeq 1.724 \times 10^8$ Pa or 25,000 psi) and at a constant temperature with a fixed gradient ($\simeq$600°C at the nutrient end and $\simeq$550°C at the seed end) for approximately 6 weeks.[6] This process is similar to quartz crystal growth except for the higher temperatures and pressures needed for KTP. Unfortunately, because of equipment restrictions, which are due to the high temperatures and pressures needed for growth, KTP crystal size is limited to approximately 20 mm × 20 mm × 60 mm, with a seed running down the middle of the crystal. Recent research aimed at optimizing nutrient composition suggests that hydrothermal growth is possible at lower temperatures (350–500°C) and pressures ($\simeq 1.4 \times 10^8$ Pa or 20,000 psi) with essentially no change in growth rate.[7] These lower temperatures and pressures will permit the use of larger autoclaves and, when the process is fully optimized, will result in the growth of significantly larger crystals.

The flux technique is essentially a high-temperature solution growth process in which the KTP crystallizes out of a molten KTP/flux composition when cooled. Depending on

0740-3224/89/040622-12$02.00

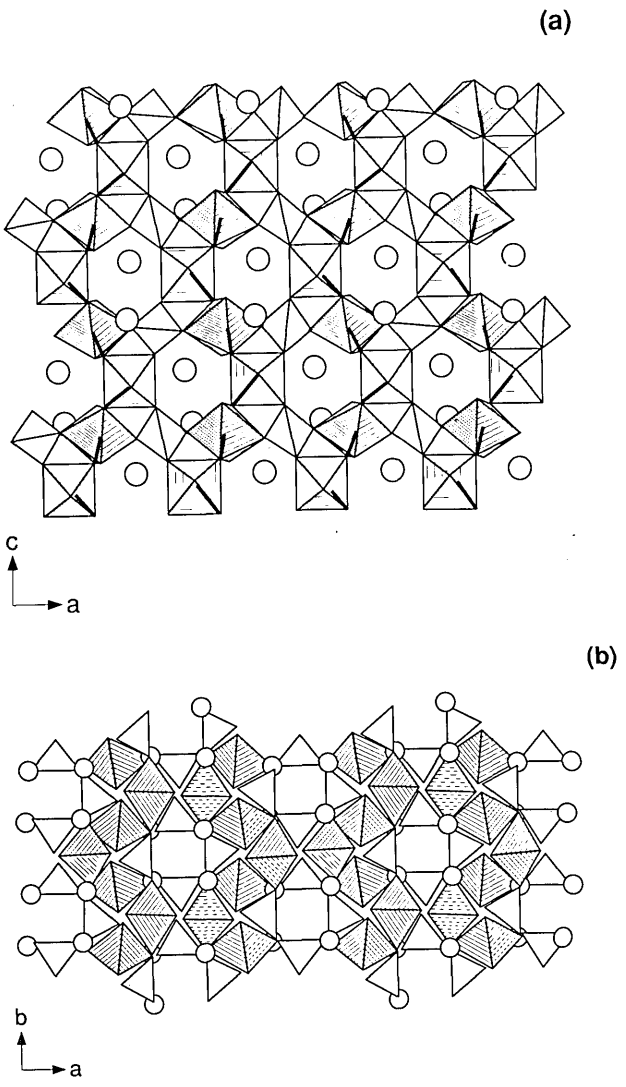

Fig. 1. KTP crystal structure: (a) a–c projection, (b) a–b projection. Shaded elements are the Ti octahedra, open elements are the P tetrahedra, and open circles are the K. The short Ti–O bonds are shown as bold lines.

the specific flux used, crystal growth can occur from approximately 700°C to approximately 1000°C, and common fluxes used are various potassium phosphates, with the K-to-P ratio varying from 1 to 3, tungstates, and halides.[8–12] A significant advantage of using the flux process is that it operates at atmospheric pressures and hence does not require sophisticated pressure equipment. However, to avoid growth striations and flux inclusions, uniform temperatures and high levels of temperature control are required. To obtain these conditions, well-insulated furnaces and heat pipes have been used.[13] Typical crystal sizes obtained to date are in the 60 mm × 55 mm × 30 mm range. Growth times vary from approximately 10 days (using a heat pipe) to 2 months (with a well-insulated furnace and good temperature control).

Because KTP belongs to the polar point group *mm*, ferroelectric domains can be present, which will decrease nonlinear-optic conversion efficiencies and increase electro-optic switching voltages. Domains have been observed in both hydrothermally grown[14] and flux grown[15] crystals. Of the various type of domain walls that have been detected, walls oriented parallel to crystallographic (100) planes are common in hydrothermally grown material. These walls have relatively low energy, and crystals with these walls can be poled at temperatures (≃500°C) that are significantly below the Curie temperature (936°C). Because the crystal-growth temperature when the hydrothermal process is used is also significantly below the Curie temperature, the use of multidomain seeds will result in the growth of multidomain crystals. In the current hydrothermal crystal-growth process only single-domain seeds are used, which ensures single-domain crystal growth. Because the flux process occurs near the Curie temperature, single-domain crystal growth is more difficult to guarantee.

The KTP crystal morphology is similar for both flux- and hydrothermal-growth processes, and specifics depend on seed size and orientation. The morphology is shown in Fig. 2 and generally consists of (100) planes, of the (201) and (011) series of planes that form relatively sharp caps along the c or polar axis, and of the (011) and (110) series of planes that form shallower caps along the b axis. Other higher-order planes can also be present, but usually these form smaller faces. The (100) planes form natural surfaces that readily cleave at room temperature when mild concentrated pressure is applied. This morphology is similar to that of KDP and has attractive properties relating to various applications. As will be discussed in Section 3, phase matching for various nonlinear processes requires propagation in the principal planes. The natural crystal morphology permits long paths and large apertures to be obtained in these directions when natural (100), (201), and (011) entrance and exit faces are used.

Although the linear-, nonlinear-, and electro-optical properties of KTP crystals grown by the flux and hydrothermal techniques are similar, differences have been observed in some of the dielectric properties and in the high-power optical-damage characteristics. From measurements done in our laboratory, the low-frequency dielectric constants,

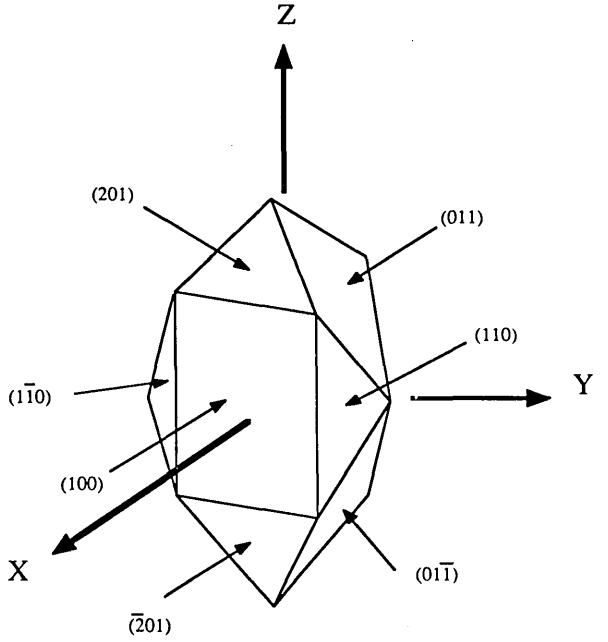

Fig. 2. Natural KTP crystal morphology.

which are dominated by K-ion conduction through a vacancy mechanism, vary over 4 orders of magnitude, depending on the growth process. Some hydrothermally grown material has very low conductivities (resistivities $>10^{11}$ Ω cm), whereas flux-grown material exhibits higher conductivities (resistivities in the 10^8-Ω cm range). The specific origins of these variations are not well known but are thought to be related to impurity ions and/or to crystal defects. Relative to optical damage, it appears that hydrothermally grown KTP has somewhat higher damage thresholds than flux-grown material. Again the origins of these differences are not understood. Some specific experimental data on damage are given in Section 3.

3. NONLINEAR-OPTICAL APPLICATIONS IN BULK KTP

KTP is a widely used material for frequency-doubling Nd:YAG lasers and other Nd-doped laser systems emitting near 1.06 μm.[16] Some of its superior properties for this important application are shown in Table 1, where some previously unpublished thermal data are also given.[17,18] Although a few specific characteristics of other materials are better, KTP has a combination of properties that make it unique for second-order nonlinear-optical applications and second-harmonic generation (SHG) of Nd lasers in particular. Its large nonlinear coefficients are phase matchable, resulting in a high figure of merit.[2,19] This property, combined with low absorption and a wide acceptance angle,[19,20] makes it the preferred doubling crystal when the available peak power is limited. The unusually large temperature bandwidth of KTP is particularly advantageous for maintaining pulsed energy stability of the converted beam.[20] The temperature bandwidth of KTP, combined with relatively good thermal properties, also gives KTP an exceptionally good figure of merit for doubling high average-power-cw or quasi-cw beams.[21] Recent experiments on intracavity frequency doubling[22,23] have also shown that KTP is much less susceptible to bulk damage than, e.g., MgO:$LiNbO_3$ at relatively high average-power levels. This property, combined with a low absorption loss at 1 μm, renders this material a prime choice for all intracavity frequency-doubling applications. Earlier observed discoloration effects (formation of gray tracks) induced by (thermal) self-focusing, causing degraded conversion efficiency followed by catastrophic damage,[24] were recently overcome by a thermal stabilization technique at temperatures above 100°C.[25] It can therefore safely be stated that KTP, with its superior qualities described above, has turned a wide variety of frequency-doubled Nd lasers into mature sources of green light.[26] Mode-locked systems emitting picosecond green pulses with >2 W of average power are now routinely used, with or without pulse-compression techniques, for synchronously or hybridly pumping other laser sources in order to generate femtosecond pulses.[27] In purely cw systems, intracavity frequency-doubled Nd:YAG lasers deliver as much as 10 W of green power[23] and have successfully replaced the Ar-ion laser as a cw pump source for tunable dye lasers used in ophthalmology.[28] Cw-pumped, intracavity-doubled, and Q-switched Nd:YAG lasers reliably generate in excess of 20-W green output.[23] These systems, which permit efficient production of high average-power UV beams (by frequency doubling the green output),[29] are now routinely used for general laser surgery.[26] Efficient intracavity-doubling of flash-lamp-pumped systems with KTP has led to the production of >10-mJ green pulses in a single transverse mode at a 10-Hz repetition rate.[30] Possible applications of this green source include the pumping of vibronic solid-state laser materials such as Ti:sapphire. In another pulsed configuration, >50% extracavity doubling efficiency has led to the generation of approximately 200 mJ in 120-μsec-long green pulses without optical damage to the doubling crystal.[31] Finally, at the low end of the power spectrum, there is an increasing interest in miniature green solid-state laser sources for a variety of applications, including optical scanning, optical data storage, laser printing, and display technology. In this category intracavity doubling of a GaAlAs diode-pumped Nd:YAG laser with a 5-mm-long KTP crystal has resulted in >10 mW of green power for only 200 mW of optical pump power (corresponding to 1 W of electrical power).[32] The overall electrical efficiency of this green laser approaches 1%. For comparison, an air-cooled ion laser operating in this region of the spectrum has a typical electrical efficiency of only 0.001%. Recent advances in intracavity-doubled miniature Nd:YAG lasers, utilizing KTP as a doubler, have led to 0.1-W green output power.[33]

Despite its proven superior qualities as a doubling crystal for 1-μm Nd lasers, only a few other applications have been addressed during the decade following the discovery of this remarkable material. Phase-matched SHG of the 1.325-μm line of Nd:YAG in KTP has been reported,[12,16] as well as sum-frequency generation of the signal and idler generated by a parametric $LiIO_3$ oscillator,[34] but few or no quantitative data are available at these wavelengths. Recently parametric downconversion near 1 μm in KTP was used for the

Table 1. Nonlinear-Optical and Thermal Properties of KTP

Property	Value
Nonlinear-optical coefficients (pm/V)	$d_{31} = 6.5$ $d_{32} = 5.0$ $d_{33} = 13.7$ $d_{24} = 7.6$ $d_{15} = 6.1$
Temperature bandwidth (°C cm)	25°
Angular bandwidth (mrad cm)[a]	15–68
Spectral bandwidth (Å cm)[a]	5.6
Walkoff (mrad)[a]	1
Temperature coefficients of refractive index ($°C^{-1}$)	$\Delta n_x = 1.1 \times 10^{-5}$ $\Delta n_y = 1.3 \times 10^{-5}$ $\Delta n_z = 1.6 \times 10^{-5}$
Transmission range (μm)	0.35–4.5
Optical absorption (%/cm)	<0.6 (at 1.064 μm) <2 (at 0.532 μm)
Thermal expansion coefficients ($°C^{-1}$)	$\alpha_1 = 11 \times 10^{-6}$ $\alpha_2 = 9 \times 10^{-6}$ $\alpha_3 = 0.6 \times 10^{-6}$
Thermal conductivity (W/cm°C)	$k_1 = 2.0 \times 10^{-2}$ $k_2 = 3.0 \times 10^{-2}$ $k_3 = 3.3 \times 10^{-2}$
Pyroelectric coefficient (nC/cm^2 °C)	7
Specific heat (cal/g °C)	0.174

[a] For SHG near 1.0 μm, propagation in the x–y plane.

Table 2. Sellmeier Equation Coefficients

Index	A	B	C	D
n_x	2.1146	0.89188	0.20861	0.01320
n_y	2.1518	0.87862	0.21801	0.01327
n_z	2.3136	1.00012	0.23831	0.01679

generation of squeezed light, both in a two-mode optical parametric oscillator[35,36] and an amplifier[37,38] configuration. One reason for the lack of interest in KTP for applicators at wavelengths other than 1 μm is that accurate Sellmeier equation fits to the refractive indices were not available, making it difficult to predict the phase-matching angles for various nonlinear interactions.[39] This is a significant problem, as it does not permit crystals to be cut properly. Recently this situation was corrected when different sets of Sellmeier equations for both flux-grown and hydrothermally grown KTP were published.[40–43] Both sets in Refs. 41 and 42 (for flux-grown KTP and both flux-grown and hydrothermally grown KTP, respectively) are constructed from a fit to observed phase-matching data. Our set[43] (for hydrothermally grown KTP), as well as the one in Ref. 40 (for flux-grown KTP), is obtained from index measurements by using the minimum deviation method. However, in Ref. 40, only 16 wavelengths between 404.7 nm and 1.064 μm were utilized; we used 47 wavelengths ranging from 350 nm to 2.4 μm. Our one-pole Sellmeier equations, with an IR correction of the form

$$n^2 = A + B/[1 - (C/\lambda)^2] - D\lambda^2, \quad (1)$$

where λ is the vacuum wavelength in micrometers and A, B, C, and D are given in Table 2, will be used in this paper. They accurately predict phase-matching angles for SHG and various sum- and difference-frequency mixing processes over the entire transparency window of hydrothermally grown KTP. (See, e.g., Refs. 43 and 44 and the angle-tuning curves given in this paper.) As an example, let us consider SHG. The exact expressions for the effective nonlinear second-order coefficients[19] d_{eff} of KTP can be simplified because of the large difference between n_z and n_x or n_y and the small difference between n_x and n_y. The approximate expression for a type-II interaction, the only efficient one, is[40]

$$d_{\text{eff}}(\text{II}) \simeq (d_{24} - d_{15})\sin 2\phi \sin 2\theta - (d_{15}\sin^2\phi + d_{24}\cos^2\phi)\sin\theta. \quad (2)$$

In Eq. (2) θ and ϕ are polar coordinates referring to the z axis and the x axis, respectively, in the x–y plane. According to Ref. 2, d_{15} = 6.1 pm/V and d_{24} = 7.6 pm/V near 1 μm. Both tensor elements have the same sign. From the Sellmeier Eq. (1), we have calculated the phase-matching angles for collinear type-II SHG in the principal planes. The results, which are summarized in Fig. 3, clearly demonstrate that type-II SHG in KTP is phase matchable over a large wavelength range. Only in the x–y plane is the birefringence too small to compensate for the dispersion in a type-II phase-matching process over a broad spectral range. According to Eq. (2) and from a glance at Fig. 3, it will be clear that phase matching in the x–z plane generally is more efficient than in the y–z plane (provided that the interaction is indeed phase matchable in both planes). The phase-matching curve $\Delta k(\alpha, \lambda) = 0$, where λ is the wavelength and α is the phase-matching angle (either θ or ϕ), shows an interesting feature. In the x–y plane the slope $[\partial(\Delta k)/\partial\alpha]$ is small; this corresponds to quasi-angle-noncritical phase matching, which ensures the double advantage of a large acceptance angle and a small walkoff angle. On the other hand, in both the x–z and the y–z planes the slope $[\partial(\Delta k)/\partial\lambda]$ is almost zero for wavelengths in the range 1.5–2.5 μm; this corresponds to quasi-wavelength-noncritical phase matching, which ensures a large spectral acceptance. Wavelength-noncritical phase matching is, of course, highly desirable for frequency conversion of short pulses. This property, however, is most often encountered in organic nonlinear-optical materials.[45] The possibilities of quasi-angle-noncritical phase matching and of wavelength-noncritical phase matching are additional advantages that make KTP attractive for applications in the near- to mid-IR region.

During the past year the availability of improved Sellmeier equations has led to the demonstration of many new applications for KTP. These include SHG of an IR dye laser down to 495 nm and sum-frequency mixing of a Nd:YAG and an IR dye laser down to 459 nm.[41,46] Angle-noncritical intracavity sum-frequency mixing of the laser (1.06 μm) and pump (809 nm) radiation in a miniature Nd:YAG laser has also been reported recently.[47] Cascade tripling of the 1.32-μm Nd:YAG line, a type-II process that is almost angle-noncritically phase matchable, has been reported to generate the shortest wavelength (440 nm) ever observed in KTP.[42] At the other end of the spectrum, the first observation of widely tunable IR generation by parametric three-photon interaction in KTP was recently reported.[43] Here we would like to report further investigations of parametric processes; we will address frequency-difference mixing applications as well.

Except for its large nonlinearity, there are several other key features that make KTP attractive for optical parametric generation (OPG), optical parametric amplification (OPA), optical parametric oscillators, and difference-frequency mixing. First, a high damage threshold (15 GW/cm^2 single shot for a 1-nsec pulse at 1.064 μm) was reported previously.[40] We measured a damage threshold of 30 GW/cm^2 at 526 nm for 30-psec pulses at a 10-Hz repetition rate in hydrothermally grown KTP and approximately a factor of 3 less for flux-grown material.[43] Second, adequate birefrin-

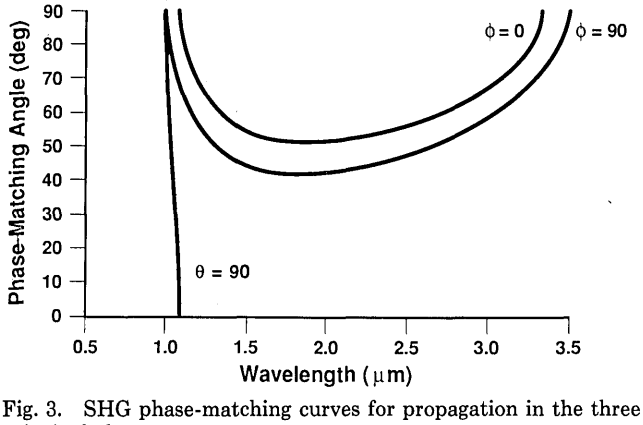

Fig. 3. SHG phase-matching curves for propagation in the three principal planes.

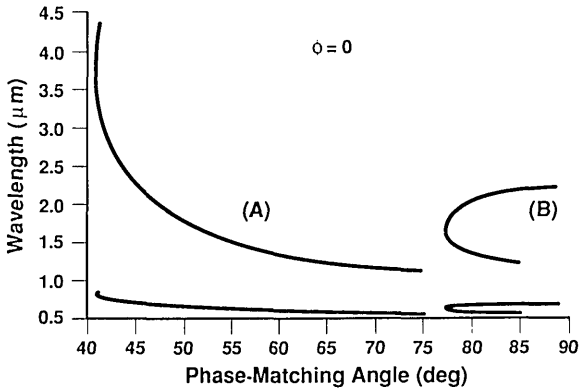

Fig. 4. Phase-matching angles for difference-frequency mixing between a tunable dye laser and the 1.053-μm radiation of a Nd:YLF laser.

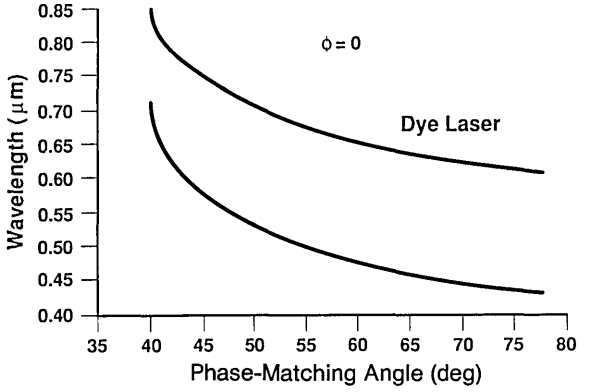

Fig. 5. Upconversion of the IR radiation shown in Fig. 4 by sum-frequency mixing with the tunable dye-laser output also shown in Fig. 4.

gence in the y-z and the x–z planes permits phase matching for the more effective type-II process over a large wavelength range, which almost covers the entire transparency window from 350 nm to 4.5 μm (with a small absorption band at 2.8 μm in hydrothermally grown crystals).[43] Finally, the existing growth and polishing methods yield sufficiently long crystals of high optical quality.

From the Sellmeier Eq. (1), we calculated phase-matching angles for difference-frequency mixing between a tunable dye laser and the 1.053-μm radiation of Nd:YLF,

$$\lambda_{dye}^{-1} - \lambda_{YLF}^{-1} = \lambda_{IR}^{-1}, \tag{3}$$

for collinear propagation in the x–z plane.[44] The results are summarized in Fig. 4. The lower curves indicate the dye-laser wavelength, and the upper curves give the corresponding IR wavelength generated by frequency-difference mixing with the 1.053-μm radiation. Sets (A) and (B) correspond to different polarization schemes: for (A) the 1.053-μm radiation is an extraordinary beam, giving rise to an ordinary IR beam; for (B) the opposite is true. The dye laser is an ordinary beam in both cases. Thus only one extraordinary beam is involved in these interactions, thereby minimizing walkoff problems. From a glance at Fig. 4, it is obvious that a large tuning range (from 1.2 to 4.4 μm) can be realized in KTP, given a dye laser that is tunable from 560 to 850 nm. Picosecond pulses in the IR with average power >1 mW at a 100-MHz repetition rate have been obtained in this way.[44] Experimental details will be given in a forthcoming publication. Mixing with the 1.32-μm radiation from Nd:YLF (or Nd:YAG) is also a possibility. For diagnostic purposes (e.g., pulse-width measurements), the IR beam generated in this way can be upconverted to the visible part of the spectrum by sum-frequency mixing (cross correlation) with the remaining dye-laser beam in KTP[44]:

$$\lambda_{IR}^{-1} + \lambda_{dye}^{-1} = \lambda_{VIS}^{-1}. \tag{4}$$

The corresponding phase-matching curve is shown in Fig. 5. Alternatively, SHG can be used in KTP for upconverting IR radiation with a wavelength in the range 1–3.4 μm, as shown in Fig. 3.

As an OPG, an OPA, or an optical parametric oscillator, KTP can most usefully be pumped by a Nd:YLF (YAG or glass) laser or its second harmonic. Obviously any other source with intermediate wavelength, such as a dye-laser oscillator–amplifier (e.g., near 600 nm), would also be a suitable pump. Figure 6 represents the calculated angle-tuning curve in the x–z plane for a 1.053-μm Nd:YLF pump (an ordinary beam):

$$\lambda_{YLF}^{-1} = \lambda_s^{-1} + \lambda_i^{-1}, \tag{5}$$

where s and i refer to signal and idler, respectively. Again, two types of interaction can take place, as is schematically indicated by (A) and (B). For (A), radiation with a wavelength longer than the degeneracy point (the idler) is polarized as an ordinary beam, and the corresponding signal is an extraordinary beam. On the other hand, for case (B), the idler is an extraordinary beam, and the signal is an ordinary beam. Obviously, type (B) has a larger d_{eff} but a narrower tunability than type (A). In both types of phase matching the tunability is large, thus making KTP attractive as a tunable near- to mid-IR source. Note the vertical slope of the tuning curves near 43° in configuration (A), indicating wavelength-noncritical phase matching (as discussed above for SHG). As a result, large bandwidths are available in this wavelength region. Because of the large nonlinearity of KTP, short crystals can be used as a parametric device, which is a distinct advantage if pulse broadening due to group-velocity dispersion has to be avoided.[48] As a combined result, the generation of mid-IR picosecond (or even subpicosecond) pulses should potentially become practical. As another example, Fig. 7 illustrates the calculated tuning

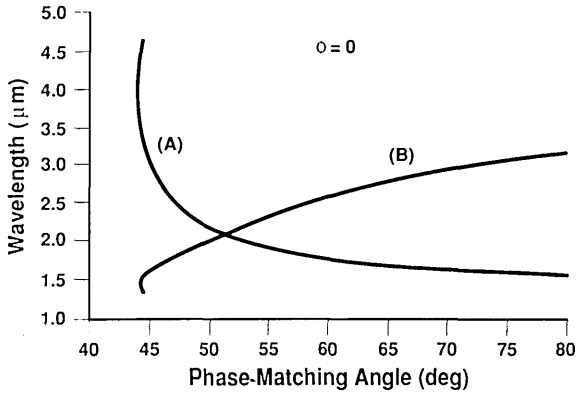

Fig. 6. Angle-tuning curve in the x–z plane for a KTP parametric generator pumped by a 1.053-μm beam.

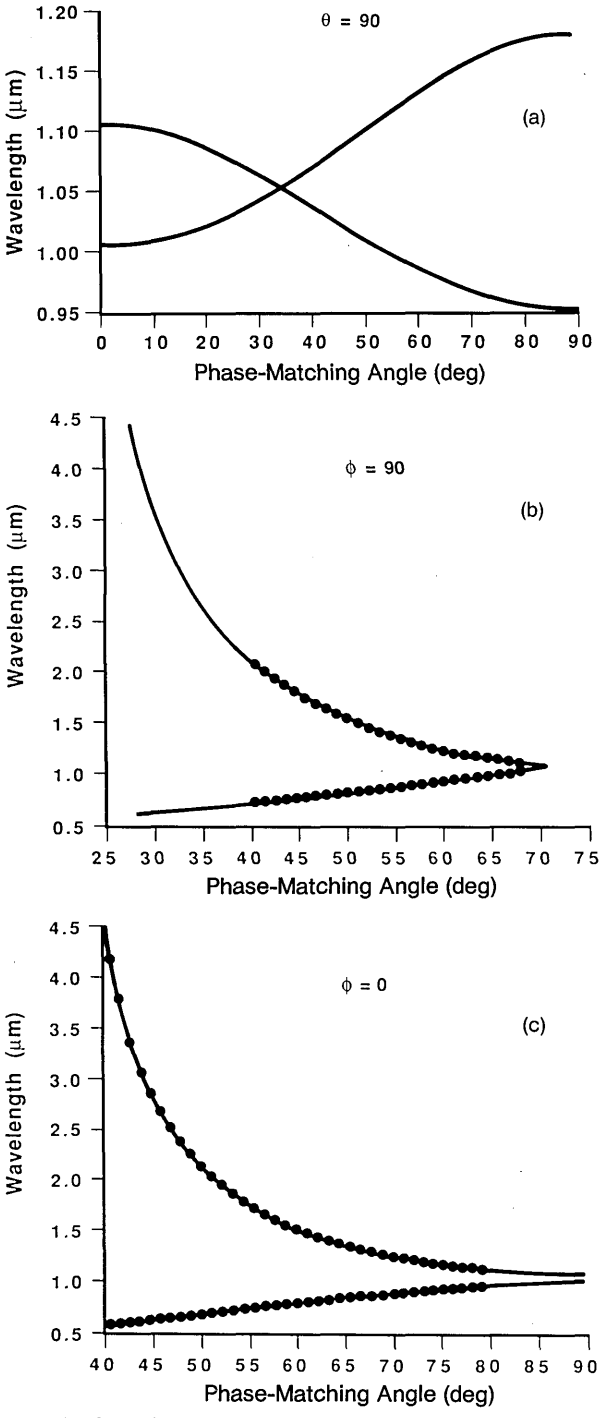

Fig. 7. Angle tuning curves in (a) the x–y plane, (b) the y–z plane, and (c) the x–z plane for a KTP parametric generator pumped by the second harmonic of a Nd:YLF laser (526 nm). The dots in (b) and (c) represent the experimental data.

curves for a 526-nm pump (second harmonic of Nd:YLF) for collinear phase matching in the x–y plane ($\theta = 90$), the y–z plane ($\phi = 90$), and the x–z plane ($\phi = 0$). Except for propagation in the x–y plane, the type-II interaction involves only one extraordinary beam (the signal beam). This means that for a single resonant optical parametric oscillator we can advantageously resonate the idler, thereby avoiding walkoff problems. From Eq. (2) and looking at Fig. 7, we can see that phase matching in the x–z plane is generally somewhat more efficient than in the y–z plane. However, phase matching in the x–z plane is not possible near the degeneracy point when we pump with the second harmonic of Nd:YLF. As a result, the tuning curve in the x–z plane has a gap from 1.007 to 1.103 μm. For many applications this small gap will not present a significant drawback. However, if fully continuous tunability is required for a 526-nm pump, phase matching in the y–z plane should be used. On the other hand, if tuning near the degeneracy point is of primary interest, we should phase match in the x–y plane. Regardless, it is clear that a broad (14 000-cm^{-1}) tuning range can be achieved with one crystal. This feature makes KTP particularly attractive as an OPG or an OPA, especially because such a device does not require any external dielectric mirrors whose bandwidths inevitably would limit the tunability.

From the Sellmeier equations, we also calculated walkoff and group-velocity dispersion effects for a 526-nm pumped crystal. The walkoff (signal beam) typically is less than 50 mrad in both the y–z and x–z planes and rapidly decreases for phase-matching angles approaching 90°. This amount of walkoff is not excessive for a crystal in which the birefringence is much larger than the dispersion and hence offers a large tuning range. The exponential amplification of a parametric process leads to signal and idler pulses that can be significantly shorter than the pump pulse, except if pulse broadening occurs as a result of group-velocity dispersion in the crystal. In KTP the difference in group velocity between, e.g., a 526-nm pump pulse and a typical signal (idler) pulse at 753 nm (1.75 μm) is approximately 1 psec/cm (5 psec/cm) for phase-matched propagation in both the y–z and x–z planes. Hence short crystals are desirable for the generation of short parametric pulses.

We have experimentally investigated OPG and OPA in KTP by using the second harmonic of a picosecond Nd:YLF system as the pump. In the past, passively mode-locked lasers were commonly used as a pump source to provide sufficiently high peak power for exponential gain.[48] However, these lasers are known to operate erratically, with large shot-to-shot fluctuations in the output energy. The more recently developed hybridly mode-locked solid-state lasers have alleviated this problem to some extent, but even these systems do not fulfill the stringent stability requirements of a parametric process.[49] We therefore used a different laser system, the details of which are described elsewhere.[25] Basically, the system consists of a cw harmonically mode-locked Nd:YLF laser that simultaneously pumps a synchronously mode-locked dye laser and seeds a Nd:YLF regenerative amplifier. The output of the regenerative amplifier is first amplified at 10 Hz in two single-pass linear amplifiers, then spatially filtered (in vacuum), and finally frequency doubled. In this way, as much as 40 mJ (at 526 nm) in a 30-psec (FWHM) pulse with a smooth Gaussian beam profile and an excellent pulse-to-pulse stability is available. On the other hand, the dye laser typically generates nearly bandwidth and diffraction-limited pulses with a duration of 1 psec (FWHM). With different sets of mirrors and a variety of dyes, this laser is tunable from 560 nm to 1.1 μm. During the course of this research, several KTP crystals were used. They were cut parallel to the natural (201) or (011) faces for propagation in the x–z or y–z planes, respectively. For both

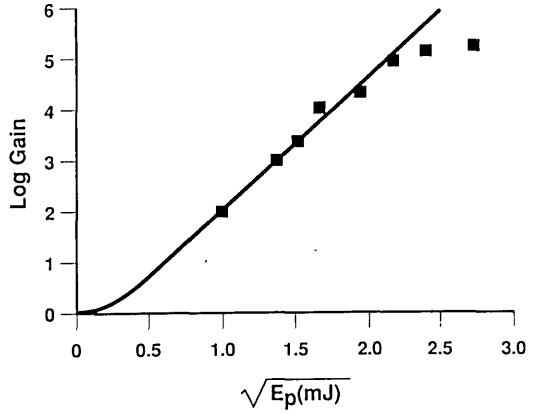

Fig. 8. Single-pass amplification at 630 nm in a 20-mm-long KTP crystal, pumped by 526 nm as a function of pump energy. The squares represent the experimental data.

cuts the normal to the entrance face makes an angle of 58.8° with the z axis. The crystals are mounted on top of a rotation stage, which permitted angular positioning with an accuracy of better than 0.5°. Frequency measurements were performed with a 0.64-m Czerny–Turner grating monochromator.

The experimentally observed angle-tuning data in the y–z plane and the x–z plane are superimposed upon the calculated curves in Fig. 7. Good agreement between calculated and observed data is obtained over the entire tuning range (600 nm–4.3 μm), thus validating the accuracy of our Sellmeier equations. For these experiments, 3-mm-long crystals were used.

To evaluate KTP as a parametric amplifier when pumped by the SHG of YLF, we carried out single-pass amplification measurements in a 20-mm-long crystal with a (201) cut. The crystal was seeded by nanojoule pulses from the dye laser tuned at $\lambda_s = 630$ nm. The corresponding idler had the wavelength $\lambda_i = 3.2$ μm. Thus amplification was studied in a less favorable case (signal and idler far from the degeneracy point at 1.053 μm and a relatively small d_{eff}). The single-pass power gain over an interaction length l, neglecting pump depletion and ignoring both linear and nonlinear absorption, is given by (MKSA units)

$$G = \cosh^2(l\Gamma), \tag{6}$$

$$\Gamma = \left(\frac{8\pi^2 I_p}{n_s n_i n_p c\epsilon_0 \lambda_s \lambda_i}\right)^{1/2} d_{\text{eff}}. \tag{7}$$

In Eq. (7) the subscripts s, i, and p refer to the signal, idler, and pump, respectively; I_p is the peak-on-axis irradiance of the pump. In the regime of strong amplification Eq. (6) reduces to the familiar result

$$G = \tfrac{1}{4}\exp(2l\Gamma). \tag{8}$$

As an example, for $l = 1$ cm and $I_p = 10$ GW/cm^2, we obtain $G = 4 \times 10^6$. Figure 8 represents the experimentally measured gain as a function of pump energy. The solid curve represents the gain calculated from Eqs. (6)–(8). From these results it is obvious that exponential amplification does indeed take place, with a saturation setting in at a pump energy of approximately 5 mJ. In this example an amplification $>10^5$ has been obtained at 630 nm with only 5 mJ per pump pulse. This is approximately what we can expect from a well-engineered dye-laser amplifier with three stages of amplification. This illustrates the great potential of KTP as an easily tunable and yet efficient parametric amplifier for (sub) picosecond pulses. The weak scatter in the experimental data illustrates the high stability of the pump source and the potential of this technique for the production of stable, tunable, high-peak-power short pulses.

OPG data obtained with 20-mm-long KTP crystals cut for propagation in the x–z plane also indicate a high-energy-conversion efficiency. With a 4-mJ pump, a single crystal typically generates 100-μJ signal pulses in the range 750–950 nm (data not corrected for Fresnel losses). Outside this range the energy of the signal pulses decreases steadily at longer wavelengths because of the gap in the phase-matching curve (see above) and at smaller wavelengths because of the combined effect of the decreasing efficiency of the parametric process if tuned away from the degeneracy point and the (weak) absorption of idler pulses near 2.8 μm. Further application of the signal (the idler) is possible by frequency-difference mixing of the idler (the signal) and the pump in a second KTP crystal. In this crystal the walkoff produced in the first crystal is compensated for. With this scheme energy-conversion efficiencies exceeding 10% have been reached. We emphasize that these are results obtained with crystals of rather poor optical quality and lacking antireflection coatings. Optical damage in KTP was not observed during the course of this research and evidently does not present a problem for this application.

Currently data for third-order $\chi^{(3)}$ nonlinear-optical properties of KTP are rather scarce. The nonlinear index of refraction n_2 of KTP has been measured and compared with those of other materials,[50] and observation of stimulated Raman scattering (SRS) in KTP has also been reported.[51] This lack of $\chi^{(3)}$ data is unfortunate, not only because $\chi^{(3)}$ properties may be useful but also because they could be limiting the efficiency of second-order processes, which involve high-peak-power radiation. For example, two-photon absorption in the green could be one of the limiting factors (other than pump depletion) responsible for the onset of saturation of the gain in the OPA configuration represented in Fig. 8. Therefore we recently started a $\chi^{(3)}$ characterization of KTP. In preliminary experiments we have observed strong stimulated polariton scattering in our 20-mm-long crystals at high pump intensities at 526 nm. The efficiently generated first and second Stokes are in agreement with earlier reports on SRS in KTP.[51] Although SRS in KTP eventually could become a practical wavelength-conversion technique, it should be noted that this effect does not compete with OPG or OPA pumped at 526 nm. This is brought about because of the differences in polarization schemes in both processes: for OPG the 526-nm pump (propagating in the x–z plane) is polarized along y, whereas for efficient SRS the pump has to be perpendicular to y. A full characterization of SRS and other $\chi^{(3)}$ properties in KTP is in progress and will be reported in a future publication.

4. ELECTRO-OPTIC AND DIELECTRIC PROPERTIES

In addition to having attractive nonlinear-optical characteristics, KTP has promising electro-optic and dielectric prop-

Table 3. Electro-Optic and Dielectric Constants of KTP

Constant	Low Frequency	High Frequency
r_{13} (pm/V)	+9.5	+8.8
r_{23} (pm/V)	+15.7	+13.8
r_{33} (pm/V)	+36.3	+35.0
r_{51} (pm/V)	7.3	6.9
r_{42} (pm/V)	9.3	8.8
r_{c1} (pm/V)	+28.6	+27.0
r_{c2} (pm/V)	+22.2	+21.5
ϵ_{11}'	11.9	11.6
ϵ_{22}'	11.3	11.0
ϵ_{33}'	>17.5	15.4

erties that make it potentially useful for various electro-optic applications. The measured electro-optic coefficients and dielectric constants are given in Table 3 and are compared with other electro-optic materials in Table 4.[3] In Table 3,

$$r_{c1} = r_{33} - (n_1/n_3)^3 r_{13} \tag{9a}$$

and

$$r_{c2} = r_{33} - (n_2/n_3)^3 r_{23} \tag{9b}$$

are the effective electro-optic coefficients used in amplitude modulation for propagation in the y and x directions, respectively. In Table 4, k is the thermal-retardation coefficient and ϵ, n, and r are the appropriate high-frequency parameters for the particular modulator configuration listed. The term n^7r^2/ϵ is a figure of merit for bulk crystal applications and corresponds to a bandwidth-to-driving-power ratio. Table 5 compares KTP with other materials for optical waveguide modulator appliations and clearly shows that KTP has a figure of merit, $n^3r/\epsilon_{\text{eff}}$, where ϵ_{eff} is the geometric average dielectric constant $(\epsilon_{11}\epsilon_{33})^{0.5}$, which is nearly 2× greater than that for the other materials listed.

The room-temperature frequency response of the electro-optic coefficient is essentially flat, except for possible piezoelectric resonances near 1–10 MHz, depending on sample cut and dimensions, from dc to the tens-of-gigahertz range. A similar frequency dependence is observed for the dielectric constants ϵ_{11} and ϵ_{22}, and the loss tangents for these two components are relatively low. However, the frequency response of the dielectric constant ϵ_{33} (both ϵ_{33}' and ϵ_{33}'') can exhibit a strong Debye-like low-frequency enhancement, depending on the crystal-growth process and the impurity level, as shown in Fig. 9. This enhancement is associated with K-ion hopping through vacancy transport and, as Fig. 9 shows, can vary from essentially no enhancement for low-temperature hydrothermally grown material[52] to enhancements of greater than 10^4 for high-temperature flux-grown material. Even for samples that show little or no enhancement at room temperature, it becomes significant at elevated temperatures when the K-ion hopping rate increases. As will be shown in Section 5, some divalent ions can readily be exchanged for K, which results in K-ion vacancy formation and in subsequent increases in the low-frequency dielectric constants (and ionic conductivity and diffusion rate).

The dc resistivity is also highly anisotropic,[3,53] generally being much lower along the polar axis, and varies considerably, depending on crystal growth and impurity in a manner similar to the low-frequency dielectric constants. In fact, this dc behavior essentially mirrors the low-frequency conductivity ($=2\pi f\epsilon''$). Resistivities measured are in the 10^8-Ω cm range for the z direction in flux-grown crystals to 10^{11}–

Table 5. Electro-Optic Waveguide Materials

	r (pm/V)	n	ϵ_{eff} $(\epsilon_{11}\epsilon_{33})^{1/2}$	$n^3r/\epsilon_{\text{eff}}$ (pm/V)
KTP	35	1.86	13	17.3
$KNbO_3$	25	2.17	30	9.2
$LiNbO_3$	29	2.20	37	8.3
$Ba_2NaNb_5O_{15}$	56	2.22	86	7.1
SBN (25–75)	56–1340	2.22	119–3400	5.1–0.14
GaAs	1.2	3.6	14	4.0
$BaTiO_3$	28	2.36	373	1.0

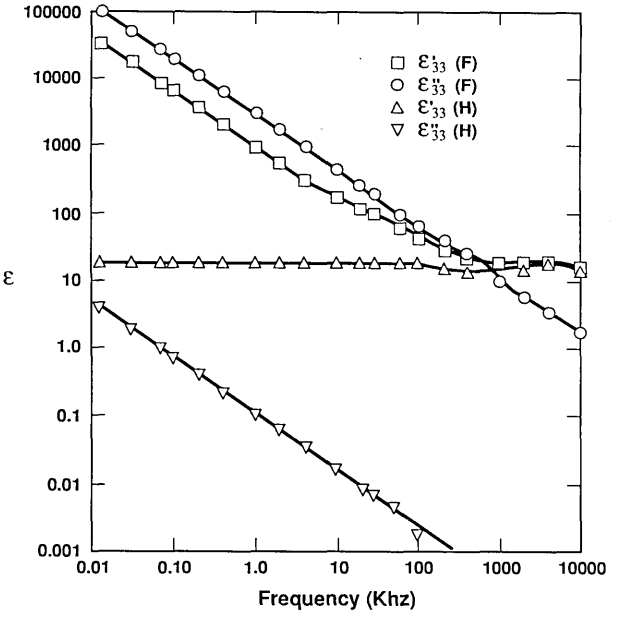

Fig. 9. Frequency dependence of dielectric constants ϵ_{33}' and ϵ_{33}'' for (F) flux-grown and (H) low-temperature hydrothermally grown KTP.

Table 4. Electro-Optic Modulator Materials

			Phase			Amplitude		
	ϵ	n	r (pm/V)	k (10^{-6}/°C)	n^7r^2/ϵ (pm/V)^2	r (pm/V)	k (10^{-6}/°C)	n^7r^2/ϵ (pm/V)^2
KTP	15.4	1.86	35.0	31	6130	27.0	11.7	3650
KD*P	48	1.47	24	9	178	24	8	178
$LiIO_3$	5.9	1.74	6.4	24	335	1.23	15	124
$LiNbO_3$	27.9	2.20	28.8	82	7410	20.1	42	3500

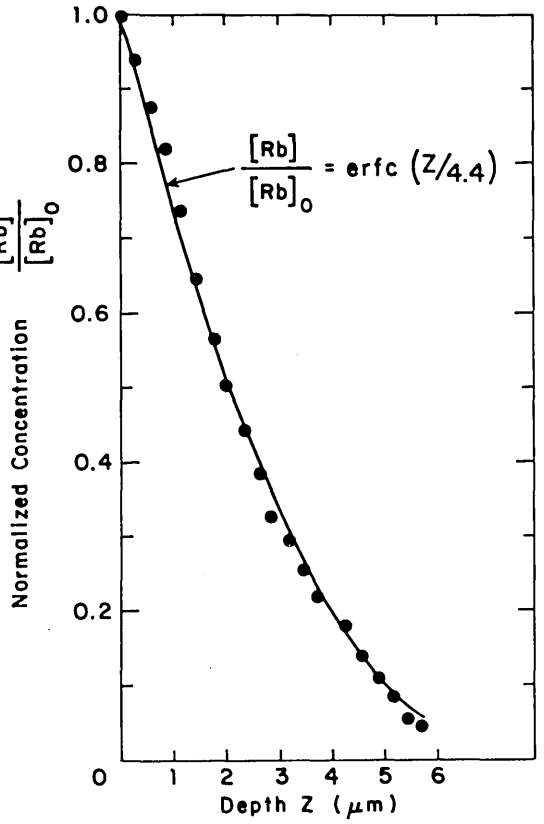

Fig. 10. Depth profile for Rb ion exchange in KTP.

10^{12} Ω cm for the x–y plane in flux-grown crystals and for all three directions in low-temperature hydrothermally grown material.

5. OPTICAL WAVEGUIDE FABRICATION AND PROPERTIES

As was shown in Section 4, KTP has an optical waveguide modulator figure of merit that is nearly 2× greater than that for any other inorganic material; hence this material should be useful for integrated-optic applications provided that low-loss optical waveguides can be fabricated. Optical waveguides have been fabricated in KTP by using an ion-exchange process that is similar to that used in forming waveguides in glass substrates.[4,54] The KTP substrates are first cut and then polished by using a process similar to that used for $LiNbO_3$ and *GGG* substrates (before liquid-phase epitaxy for magnetic bubble memories). For fabricating channel waveguides, a suitable metal mask (e.g, Al, Au, Ti) is applied to the polished surface. This mask has a pattern with open areas where the waveguide is wanted. The ion-exchange bath consists of a molten nitrate salt of Rb, Cs, or Tl or various mixtures of these salts heated to between 300°C and 400°C. The masked KTP is immersed in the bath for the time required to form the waveguide, typically 30 min–4 h.

The waveguides formed in this way have an exchanged-ion concentration depth profile (and refractive-index profile) that is close to a complementary error-function distribution, as is expected for a diffusion-controlled process. A typical depth profile, measured using an electron microprobe, for a Rb-exchanged guide is shown in Fig. 10, which clearly shows the error-function distribution. Figure 11 shows a phase-contrast photomicrograph of a 6-μm-wide channel Tl-exchanged waveguide. Note the sharp boundaries at the edge of the guide and the uniformity across the guide. A summary of the refractive indices that can be induced by the various exchanged ions, optical attenuation, and process conditions are given in Table 6. All the results given in this table are for z-cut substrates. Because the ion-exchange rate or diffusion constant for the Rb, Cs, and Tl ion-exchange processes is several orders of magnitude greater in the z direction than in the x–y plane, devices requiring well-defined channels will be restricted to z-cut substrates.

Because the ion-exchange rate depends on substrate ionic conductivity, variations in conductivity will result in variations in waveguide properties. Such variations have been observed, and they have caused some problems with device fabrication. To improve the guide uniformity and reduce the effects of variations in substrate conductivity, we added a divalent ion salt to the monovalent nitrate salt bath. For

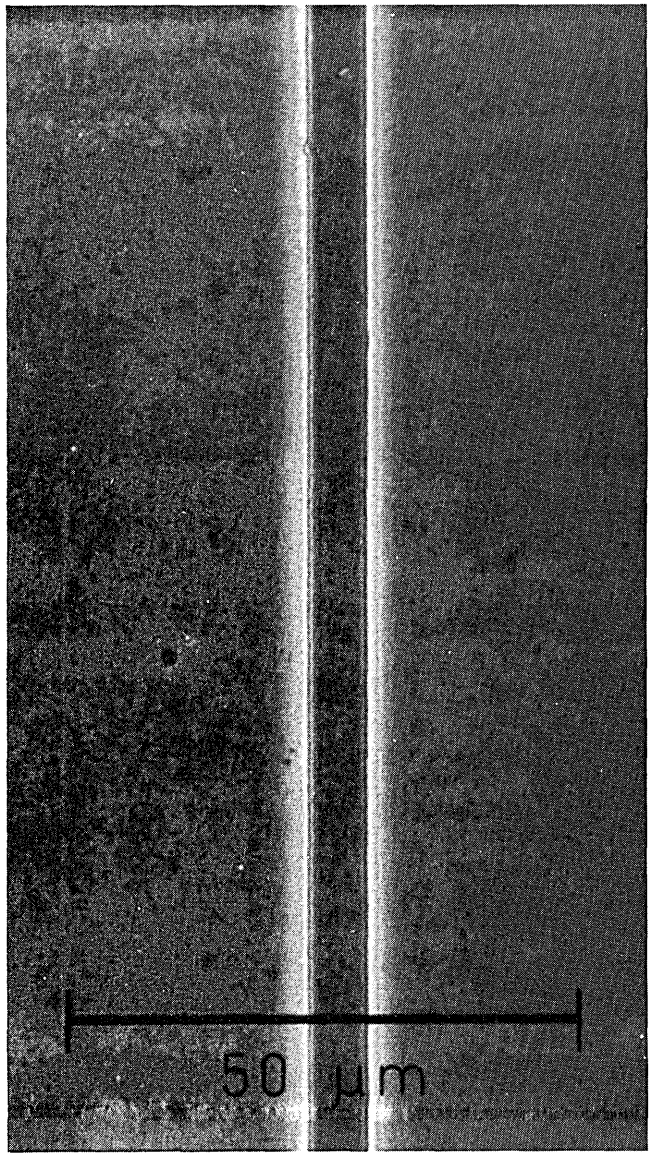

Fig. 11. Top view of a Tl-exchanged channel waveguide in KTP.

Table 6. Ion-Exchanged Waveguides in $KTiOPO_4$

Process	
Salts:	$RbNO_3$, $CsNO_3$, $TlNO_3$
Temp:	315–400°C
Time:	0.5–4.0 h
Surface Refractive-Index Increase ($\Delta n_x = \Delta n_y = \Delta n_z$)	
Rb:	$\Delta n = 0.020$
Cs:	$\Delta n = 0.023$
Ti:	$\Delta n = 0.23$
Attenuation (Rb, Tl)	<0.4 dB/cm

Table 7. Effect of Divalent Ion on KTP Waveguide Properties (Rb^+/M^{++} Ion Exchange, 300°C, 2 h)

M	Ionic Radii (Å)	Depth (μm)	Δn
None (325°C)	–	0	0
Ca	1.18	1	0.007
Sr	1.30	7	0.018
Ba	1.47	15	0.025
K	1.55		

ions of the appropriate ionic radii, small amounts of the divalent ion will substitute for K in the KTP lattice, resulting in the formation of K-ion vacancies. These vacancies increase the ionic conductivity near the surface, which increases the monovalent ion-exchange rate and hence reduces the effect of variations in substrate conductivity. The alkaline-earth ions have the appropriate ionic radii to substitute for K, and the results of forming waveguides by using these ions (20 mol %) with Rb are shown in Table 7. As is obvious from this table, the effectiveness of the divalent ion, which corresponds to a divalent-ion–K-ion exchange rate, increases as its ionic radius approaches that of K. For this particular substrate, without the divalent-ion salt addition, essentially no waveguides are formed, even at a higher exchange temperature.

An example of the effectiveness of the divalent ion on the exchange rate is shown in Fig. 12. Here a 20/80 $Ba(NO_3)_2$/$RbNO_3$ (molar ratio) bath was used, and the KTP sample was treated at 350°C for 2 h. The waveguide depth is nearly 100 μm. Without the Ba salt the waveguide depth would vary from less than 1 to approximately 8 μm, depending on substrate conductivity. Figure 12 also shows the effect of the highly anisotropic diffusion properties of KTP. Essentially no latteral diffusion is observed for this 6-μm-wide channel waveguide, although it is approximately 100 μm deep. Such an anisotropic diffusion characteristic will have potentially significant device advantages, such as in fabricating high-density guide arrays, optimizing electric-field overlap for modulators and switches, optimizing optical-field overlap for nonlinear waveguide devices, and fabricating modulated index guides.

6. WAVEGUIDE DEVICES AND APPLICATIONS

KTP has several potential advantages for optical waveguide devices compared with other materials in addition to having a much larger modulator figure of merit. Its high optical-damage threshold suggests that KTP waveguide devices could be used to control or convert high-intensity optical beams with input wavelengths extending from the visible to the IR. Also, KTP waveguide devices should be much less susceptible to piezoelectric and pyroelectric instabilities because these effects have not been observed in bulk device applications, and hence device thermal and mechanical stability should be much better.

Several demonstration electro-optic and nonlinear-optic devices have been fabricated by using KTP with the above waveguide fabrication process. The measured V_π for several single-channel phase modulators that have been fabricated indicates that the waveguide fabrication process does not alter the electro-optic coefficient. Using a 6-μm-wide channel waveguide and a 0.2-μm MgF_2 buffer layer, and coupling to the r_{c2} electro-optic coefficient, we observed a $V_\pi l$ of 6 V cm at 6328 Å, which is close to the theoretically predicted value for KTP's bulk electro-optic and dielectric constants.[54] These devices are dc stable for both hydrothermally and flux-grown substrates. In some devices the $V_\pi l$ was lower than 6 V cm at low frequencies and increased to 6

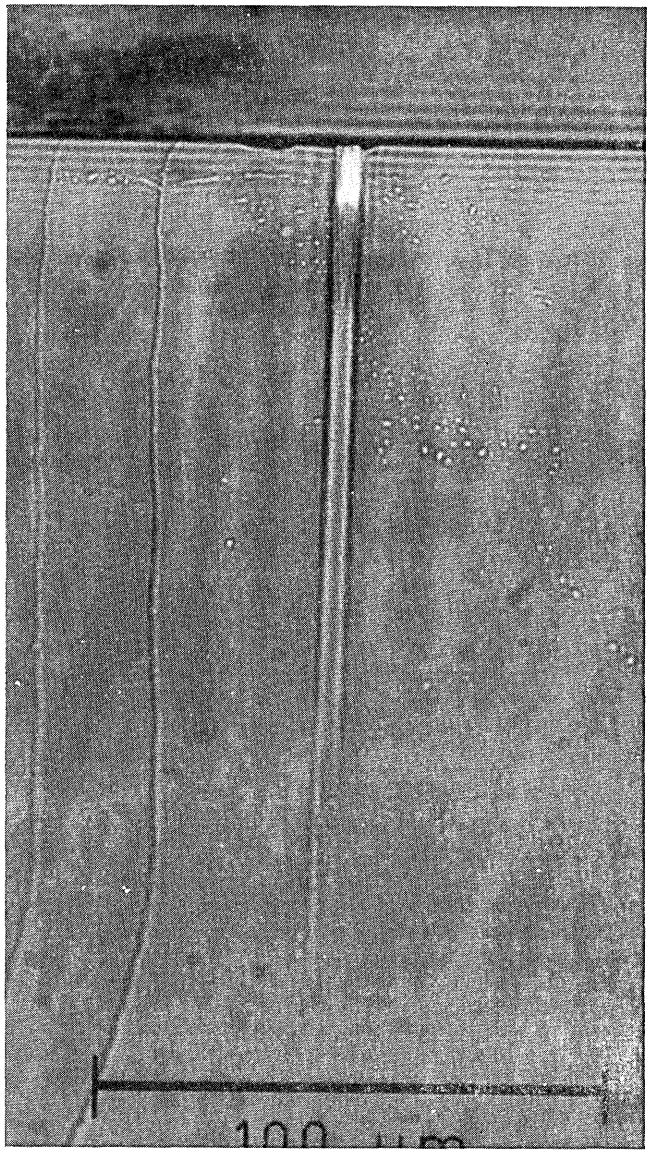

Fig. 12. End view of a Ba/Rb-exchanged channel waveguide in KTP.

V cm at high frequency. Evidently, some ionic-conduction effects are occurring in these samples, which suggests that the dc conductivity of the Rb-rich optical waveguide is lower than that of bulk KTP. Limited data on the dielectric properties of bulk $RbTiOPO_4$ indicate such a lower conductivity, a result that is not totally unexpected because Rb has a larger ionic radius compared with K, giving a lower ion hopping rate.

A Mach–Zehnder modulator was also fabricated on a 1-mm-thick, z-cut KTP substrate by using 6-μm-wide Rb-exchanged waveguides and traveling-wave electrodes that show a bandwidth of nearly 16 GHz.[55] This modulator was fabricated with a 0.4-μm SiO_2 buffer layer, a 1-cm electric-field interaction length, and a 25-μm electrode gap and had a V_π of 10 V at a 1.3-μm input wavelength and 5 V at 0.633 μm. In addition to being dc-bias and thermally stable, this modulator did not show any instabilities due to optical damage or photorefraction, which are commonly observed in other materials, even with inputs of as great as 1 mW.

The nonlinear-optical properties of KTP waveguides have also been evaluated by measuring the SHG output, using a diode-pumped Nd:YAG input at 1.064 and 1.31 μm. Using a 6-μm-wide Rb-exchanged channel waveguide, we measured conversion efficiencies to the green in the 4% W^{-1} cm^{-2} range.[56] (Conversion efficiencies given have been normalized to input power in the guide and to guide length.) This conversion efficiency is close to the best values measured (4.8%) for Ti:$LiNbO_3$ waveguides. At 1.31-μm input we recently measured conversion efficiencies of approximately 1% W^{-1} cm^{-2}. Additional experiments aimed at evaluating parametric processes, using resonant structures and extending the phase matching to shorter wavelengths, are ongoing.

7. CONCLUSIONS

We have reviewed the crystal structure and crystal growth of KTP and its linear- and nonlinear-optic, electro-optic, dielectric, and optical waveguide properties. KTP is an important material for SHG of the Nd:YAG and other Nd:doped lasers and has been shown to have attractive properties for sum- and difference-frequency mixing and OPG. It also has large electro-optic coefficients and low dielectric constants that make it potentially useful for integrated-optic applications as well. Low-loss optical waveguides can be formed in KTP by using a relatively simple ion-exchange technique. These guides have high optical-damage resistance, are thermally stable, can be fabricated with refractive-index increases as great as 0.23, and have electro-optic properties similar to bulk material. Several optical waveguide electro-optic and nonlinear-optic demonstration devices have been fabricated. These devices confirm that KTP is also a superior material for many optical waveguide applications.

ACKNOWLEDGMENTS

We acknowledge the valuable contributions of J. B. Brown for substrate preparation and waveguide fabrication and evaluation, of J. H. Kelly for aid in the optical parametric evaluations, of S. A. Burroughs for aid in the waveguide fabrication, and of W. Y. Hsu and G. R. Meredith for their support and encouragement.

REFERENCES

1. J. D. Bierlein and T. D. Gier, U.S. Patent 3,949,323 (April 6, 1976).
2. F. C. Zumsteg, J. D. Bierlein, and T. E. Gier, "$K_xRb_{1-x}TiOPO_4$: a new nonlinear optical material," J. Appl. Phys. **47**, 4980 (1976).
3. J. D. Bierlein and C. B. Arweiler, "Electro-optic and dielectric properties of $KTiOPO_4$," Appl. Phys. Lett. **49**, 917 (1986).
4. J. D. Bierlein, A. Ferretti, L. H. Brixner, and W. Y. Hsu, "Fabrication and characterization of optical waveguides in $KTiOPO_4$," Appl. Phys. Lett. **50**, 1216 (1987).
5. I. Tordjman, R. Masse and J. C. Guitel, "Structure cristalline du monophosphate $KTiPO_5$," Z. Kristallogr. **139**, 103 (1974).
6. G. Gashurov and R. F. Belt, "Growth of KTP," in *Tunable Solid State Lasers for Remote Sensing*, R. L. Byer, E. K. Gustafson, and R. Frebino, eds. (Springer-Verlag, New York, 1985), p. 119.
7. R. A. Laudise, R. J. Cava, and A. J. Caporaso, "Phase relations, solubility and growth of potassium titanyl phosphate, KTP," J. Crystal Growth **74**, 275 (1986).
8. D. F. Cai and Z. T. Yang, "Investigation on some properties of $KTiOPO_4$ crystals," J. Crystal Growth **79**, 974 (1986).
9. D. Z. Shen and C. E. Huang, "A new nonlinear optical crystal KTP," Prog. Crystal Growth Characterization **11**, 269 (1985).
10. J. C. Jacco, G. M. Loiacono, M. Jaso, G. Mizell, and B. Greenberg, "Flux growth and properties of $KTiOPO_4$," J. Crystal Growth **70**, 484 (1984).
11. Y. G. Liui, B. Xu, J. R. Han, X. Y. Liu, and M. H. Jiang, "Growth of $KTiOPO_4$ crystal for high efficiency SHG devices and its main properties," Chin. J. Lasers **13**, 438 (1986).
12. A. A. Ballman, H. Brown, D. H. Olson, and C. E. Rice, "Growth of potassium titanyl phosphate (KTP) from molten tungstate melts," J. Crystal Growth **75**, 390 (1986).
13. P. F. Bordui, J. C. Jacco, G. M. Loiacono, R. A. Stolzenberger, and J. J. Zola, "Growth of large single crystals of $KTiOPO_4$ (KTP) from high-temperature solution using heat pipe based furnace system," J. Crystal Growth **84**, 403 (1987).
14. J. D. Bierlein and F. Ahmed, "Observation and poling of ferroelectric domains in $KTiOPO_4$," Appl. Phys. Lett. **51**, 1322 (1987).
15. G. M. Loiacono and R. A. Stolzenberger, "Observations of complex domain walls in $KTiOPO_4$," Appl. Phys. Lett. **53**, 1498 (1988); V. I. Voronkova, R. S. Gvozdover, and V. K. Vanovskii, "Ferroelectric domains in $KTiOPO_4$ and $RbTiOPO_4$ crystals," Sov. Tech. Phys. Lett. **13**, 390 (1987).
16. R. F. Belt, G. Gashurov, and Y. S. Liu, "KTP as a harmonic generator for Nd:YAG lasers," Laser Focus **21**, 110 (1985).
17. F. C. Zumsteg, E. I. du Pont de Nemours & Company, Wilmington, Delaware 19880 (personal communicaton).
18. T. E. Gier and F. C. Zumsteg, "KTP crystals for second harmonic generation," written for contract F33615-77-C-1131 (E. I. du Pont de Nemours & Company, Wilmington, Del., November 1978).
19. J. Q. Yao, and T. S. Fahlen, "Calculations of optimum phase match parameters for the biaxial crystal $KTiOPO_4$," J. Appl. Phys. **55**, 65 (1984).
20. Y. S. Liu, L. Drafall, D. Dentz, and R. Belt, "Nonlinear optical phase-matching properties of $KTiOPO_4$," Technical Information Series Rep. 82CRD016 (General Electric, Schenectady, N.Y., 1982).
21. D. T. Hon, "High average power, efficient second harmonic generation," in *Laser Handbook*, M. L. Stitch, ed. (North-Holland, New York, 1979), Vol. 3, p. 421.
22. Y. S. Liu, D. Dentz, and R. Belt, "High-average-power intracavity second-harmonic generation using $KTiOPO_4$ in an acousto-optically Q-switched Nd:YAG laser oscillator at 5 kHz," Opt. Lett. **9**, 76 (1984).
23. P. E. Perkins, and T. S. Fahlen, "20-W average-power KTP intracavity-doubled Nd:YAG laser," J. Opt. Soc. Am. B **4**, 1066 (1987).
24. T. A. Driscoll, H. J. Hoffman, R. E. Stone, and P. E. Perkins, "Efficient second-harmonic generation in KTP crystals," J. Opt. Soc. Am. B **3**, 683 (1986).
25. H. Vanherzeele, "Optimization of a cw mode-locked and frequency-doubled Nd:YLF laser," Appl. Opt. **27**, 3608 (1988).

26. G. Huth and D. Kuizenga, "Green light from doubled Nd:YAG lasers," Lasers Optron. **6,** 59 (1987).
27. See, e.g., D. A. Auston and K. B. Eisenthal eds., *Proceedings of the Conference on Ultrafast Phenomena IV,* (Springer-Verlag, Berlin, 1984); G. R. Fleming and A. E. Siegman, eds., *Proceedings of the Conference on Ultrafast Phenomena V* (Springer-Verlag, Berlin, 1986).
28. H. Vanherzeele, L. De Vos, and P. Muys, "Tunable dye laser pumped by a frequency-doubled high power cw Nd:YAG laser," J. Opt. Soc. Am. A **3** (13), P65 (1986).
29. P. E. Perkins and T. S. Fahlen, "Half watt average power at 25 kHz from fourth harmonic of Nd:YAG," IEEE J. Quantum Electron. **QE-21,** 1636 (1985).
30. P. E. Perkins and T. A. Driscoll, "Efficient intracavity doubling in flash-lamp pumped Nd:YLF," J. Opt. Soc. Am. B **4,** 1281 (1987).
31. S. E. Moody, J. M. Eggleston, and J. F. Seamans, "Long-pulse second harmonic generation in KTP," IEEE J. Quantum Electron. **QE-23,** 335 (1987).
32. T. Baer, "Frequency-doubled, diode pumped Nd:YAG lasers," Proc. Soc. Photo-Opt. Instrum. Eng. **610,** 45 (1986).
33. P. Kortz, Adlas GmbH, Lubeck, Federal Republic of Germany (personal communication).
34. A. L. Aleksandrovskii, S. A. Akhmanov, V. A. D'yakov, N. I. Zheludev, and V. I. Pryalkin, "Efficient nonlinear optical converters made of potassium titanyl phosphate crystals," Sov. J. Quantum Electron. **15,** 885 (1985).
35. S. Reynaud, C. Fabre, and E. Giacobino, "Quantum fluctuations in a two-mode parametric oscillator," J. Opt. Soc. Am. B **4,** 1520 (1987).
36. A. Heidmann, R. J. Horowicz, S. Reynaud, E. Giacobino, and C. Fabre, "Observation of quantum noise reduction of twin laser beams," Phys. Rev. Lett. **59,** 2555 (1987).
37. P. Grangier, R. E. Slusher, B. Yurke, and A. LaPorta, "Squeezed light-enhanced polarization interferometer," Phys. Rev. Lett. **59,** 2153 (1987).
38. R. E. Slusher, P. Grangier, A. LaPorta, B. Yurke, and M. J. Potasek, "Pulsed squeezed light," Phys. Rev. Lett. **59,** 2566 (1987).
39. K. H. Hellwege, ed., *Landolt–Bornstein Tables,* Nonlinear Dielectric Susceptibilities (Springer-Verlag, Berlin, 1979), Vol. 2, Group 3, Sec. 6.; Sellmeier equations in this reference are constructed from only a limited refractive-index data set from Ref. 2 for hydrothermally grown KTP.
40. T. Y. Fan, C. E. Huang, B. Q. Hu, R. C. Eckardt, Y. X. Fan, R. L. Byer, and R. S. Feigelson, "Second harmonic generation and accurate index of refraction measurements in flux-grown $KTiOPO_4$," Appl. Opt. **26,** 2390 (1987).
41. K. Kato, "Second harmonic and sum-frequency generation to 4950 and 4589 Å in KTP," IEEE J. Quantum Electron. **QE-24,** 3 (1988).
42. D. W. Anthon and C. D. Crowder, "Wavelength dependent phase matching in KTP," Appl. Opt. **27,** 2650 (1988).
43. H. Vanherzeele, J. D. Bierlein, and F. C. Zumsteg, "Index of refraction measurements and parametric generation in hydrothermally-grown $KTiOPO_4$," Appl. Opt. **27,** 3314 (1988).
44. H. Vanherzeele, "Optical parametric conversion of picosecond pulses in $KTiOPO_4$," J. Opt. Soc. Am. A **5**(13), P87 (1988).
45. I. Ledoux, J. Badan, and J. Zyss, "Generation of high-peak power tunable infrared femtosecond pulses in an organic crystal: application to time resolution of weak infrared signals," J. Opt. Soc. Am. B **4,** 987 (1987).
46. J.-C. Baumert, F. M. Schellenberg, W. Lenth, W. P. Risk, and G. C. Bjorklund, "Generation of blue cw coherent radiation by sum frequency mixing in $KTiOPO_4$," Appl. Phys. Lett. **51,** 2192 (1987).
47. W. P. Risk, J.-C. Baumert, G. C. Bjorklund, F. M. Schellenberg, and W. Lenth, "Generation of blue light by intracavity frequency mixing of the laser and pump radiation of a miniature neodymium:yttrium aluminum garnet laser," Appl. Phys. Lett. **52,** 85 (1988).
48. A. Seilmeier and W. Kaiser, "Generation of tunable picosecond light pulses covering the frequency range between 2,700 and 32,000 cm^{-1}," Appl. Phys. **23,** 113 (1980).
49. D. W. Anthon, H. Nathel, D. M. Guthals, and J. H. Clark, "Scanning picosecond optical parametric source using potassium dihydrogen phosphate in the visible and near infrared," Rev. Sci. Instrum. **58,** 2054 (1987).
50. L. L. Chase, R. Adair, and S. A. Payne, "Influence of structure and composition of the third-order susceptibility of inorganic optical materials," Mat. Res. Soc. **EA-12,** 13 (1987).
51. G. A. Massey, T. M. Loehr, L. J. Willis, and J. C. Johnson, "Raman and electrooptic properties of potassium titanate phosphate," Appl. Opt. **19,** 4136 (1980).
52. R. F. Belt, G. Gashurov, and R. A. Laudise, "Low temperature hydrothermal growth of $KTiOPO_4$ (KTP)," Proc. Soc. Photo-Opt. Instrum. Eng. **968,** 100 (1988).
53. V. K. Yanovskii and V. I. Voronkova, "Ferroelectric phase transitions and properties of crystals of the $KTiOPO_4$ family," Phys. Status Solidi A **93,** 665 (1986).
54. J. D. Bierlein, A. Ferretti, and M. Roelofs, "$KTiOPO_4$ (KTP): a new material for optical waveguide applications," Proc. Soc. Photo-Opt. Instrum. Eng. **994,** 160 (1989).
55. D. B. Laubacher, V. L. Guerra, M. P. Chouinard, J.-Y. Liou, and P. H. Wyat, "Fabrication and performance of KTP optoelectronic modulators," Proc. Soc. Photo-Opt. Instrum. Eng. **993,** 80 (1988).
56. J. D. Bierlein, "Nonlinear wavelength conversion in $KTiOPO_4$ waveguides," in *Proceedings of the International Meeting on Advanced Materials* (Materials Research Society, Pittsburgh, Pa., 1989).